Constraining the dark energy-dark matter interaction model using low-redshift observations

Archana Sangwan*, Joseph P J†, and S. Shankaranarayanan‡
Department of Physics, Indian Institute of Technology Bombay, Mumbai 400076, India
* *E-mail: arch06san@gmail.com,* † *E-mail: josephpj@iitb.ac.in*
‡ *E-mail: shanki@phy.iitb.ac.in*

Various observations have shown that dark energy accounts for nearly two-thirds of the energy density of the Universe. The simplest model to explain the nature of dark energy is the cosmological constant (ΛCDM) model. Although Planck observations supports using ΛCDM model as the base cosmological model, there exist some inconsistencies in parameter estimates when compared with independent observations. The most important is the inconsistency in the H_0 estimates from the Planck collaboration which reports $H_0 = 67.5^{+0.5}_{-0.5}\ km\ s^{-1}\ Mpc^{-1}$, a considerably lower value when compared with the direct local distance ladder measurements. This value shows a discrepancy at the level greater than 4σ with the constraints reported by SH0ES collaboration in 2019, $H_0 = 74.3^{+1.42}_{-1.42}$ $km\ s^{-1}\ Mpc^{-1}$. These disagreements, called the Hubble tension, point towards a new physics that deviates from the standard ΛCDM model and to resolve this various methods have been proposed. In this work, a quintessence scalar field with an inverse power potential ($V(\phi) \sim \phi^{-n}$) is assumed as a description of dark energy and we focus on an interacting dark energy dark matter model where the interacting term is taken to be linear in the field (Φ). We study in detail the evolution of the model and provide constraints on the model parameters using low redshift cosmological observations of Type Ia Supernovae (SN), baryon acoustic oscillations (BAO), direct measurements of Hubble parameter (Hz) and high redshift HII galaxy measurements (HIIG). We find that the model agrees with the existing values of the nonrelativistic matter density parameter, Ω_m and dark energy equation of state parameter, w_0. The analysis shows that the observations prefer a negative value of coupling constant and gives the best fit value of $H_0 = 69.9^{+0.46}_{-1.02}\ km\ s^{-1}\ Mpc^{-1}$ and thereby can be used to alleviates the H_0 tension between Planck measurements and the observations considered.

Keywords: Cosmological parameter, observations, dark energy - dark matter interaction, based on the work [arXiv:2102.12367].[1]

1. Introduction

Many cosmological observations suggest that, at the present epoch, the energy content of the universe is dominated by dark energy, and to explain the observed accelerated expansion of the universe, this dark energy component must have a negative pressure.[2–5] However, the nature of dark energy is still a mystery, and many models are proposed in the literature to explain what dark energy might be. The simplest model is the ΛCDM model, which is also the most consistent model for cosmological observations. The latest results from the Planck mission provide good support to the ΛCDM model as the base cosmological model and also improve upon the uncertainties in parameter estimation.[6,7] With more accurate and precise measurements, the

uncertainties from various experiments have been studied and are in disagreement with each other. The most glaring tension is found in the estimation of the Hubble parameter reported by the Planck collaboration and the low redshift cosmological probes.[8–10] In some cases, the tension stands at level greater than 4σ, e.g., Planck 2018 results, which assume standard ΛCDM model as the base cosmological model, report Hubble parameter to be $H_0 = 67.4 \pm 0.5\ km\ s^{-1}\ Mpc^{-1}$,[7] whereas SH0ES collaboration estimates $H_0 = 73.5 \pm 1.4\ km\ s^{-1}\ Mpc^{-1}$.[11] Another discrepancy, although not as severe, is found in the estimation of σ_8 reported by Planck 2018 and low redshift observation with stands at a level of 2σ-3σ level.[12–17] The high precision of the data from Planck collaboration and low redshift probes insinuate that the H_0 tension between these experiments cannot result from the systematics and hence, points towards a new physics that deviates from the standard ΛCDM model.

Many models have been proposed and studied to resolve these disagreements in literature. One such proposal is to consider a non-zero interaction between dark energy and dark matter which could alleviate these disagreements.[18–21] In this work, we focus on an interacting dark sector model, which is introduced in.[22] In most cases, this interaction term is introduced in fluid equations by hand, which might not be consistent with the classical field theory action. In the Ref.,[22] instead of putting it by hand, the authors derive the interaction term, which is consistent with both fluid descriptions and classical field theory description. We use this interaction term in our work and study whether the interaction model is consistent with low redshift observations such as direct measurement of Hubble parameter (Hz),[23–28] measurements of HII galaxy (HIIG),[29,30] baryon acoustic oscillations (BAO),[31–36] and type Ia supernovae (SN).[37] We constrain the model parameters, and after analyzing, find that using only the background observations, we cannot distinguish between interacting and noninteracting scenarios. Two see a clear distinction between the two cases; we have to study the evolution of perturbed quantities.

2. Dark Energy Dark Matter Interaction Model

The interacting model is described by the action

$$S = \int d^4x\sqrt{-g}\left(\frac{1}{2\kappa^2}R - \frac{1}{2}g^{\mu\nu}\nabla_\mu\phi\nabla_\nu\phi - U(\phi) - \frac{1}{2}e^{2\alpha(\phi)}g^{\mu\nu}\nabla_\mu\chi\nabla_\nu\chi - e^{4\alpha(\phi)}V(\chi)\right). \tag{1}$$

where dark energy is denoted by the scalar field ϕ, $U(\phi)$ is the scalar field potential, dark matter is represented by the scalar fieldχ, and $\alpha(\phi)$ denotes the dark energy dark matter interaction (For more details, see[22]).

The Einstein equation in terms of the scalar field (ϕ) and dark matter fluid, specified by four-velocity energy density and pressure, is given by[22]

$$G_{\mu\nu} = 16\pi G\left[\nabla_\mu\phi\nabla_\nu\phi - \frac{1}{2}g_{\mu\nu}\nabla^\sigma\phi\nabla_\sigma\phi - g_{\mu\nu}V(\phi) + p_m g_{\mu\nu} + (\rho_m + p_m)u_\mu u_\nu\right], \tag{2}$$

and the energy-momentum tensor for the dark matter fluid is given by

$$T_\nu^{(m)\mu} = p_m g_{\mu\nu} + (\rho_m + p_m) u_\mu u_\nu \,. \tag{3}$$

The interaction term is described by $\nabla_\mu T_\nu^{(m)\mu} = Q_\nu^{(\mathrm{F})}$, and by demanding that the interaction term Q_ν must have a field theory description, they obtained a unique form of interaction term, given by[22]

$$Q_\nu^{(\mathrm{F})} = T^{(m)} \nabla_\nu \alpha(\phi) \,. \tag{4}$$

We study the evolution of cosmological equations in the presence of the interaction and obtain constraints on the model parameters by assuming a specific form of scalar field potential and the interaction term. In this work, we assume a quintessence scalar field described by the inverse power law potential and an interaction term that is linear in the field (ϕ),

$$U(\phi) \sim \frac{1}{\phi^n}, \qquad n \;=\; 1, 2, \tag{5}$$

$$\alpha(\phi) \sim \phi, \qquad \alpha(\phi) = C\phi \tag{6}$$

where C is the interaction strength. The evolution of the scalar field is described by the Klein-Gordon equation given by

$$(\ddot{\phi} + 3H\dot{\phi} + U_{,\phi})\dot{\phi} = Q \,,$$

where $Q = Q_0^{(\mathrm{F})}$. The scalar field potential in terms of dimensionless parameter $\tilde{\phi}$ is

$$U(\tilde{\phi}) = \frac{\kappa}{2}\, m_{\mathrm{Pl}}^2 \tilde{\phi}^{-n} \tag{7}$$

where κ is a constant and m_{Pl}, is the Planck mass. The evolution of non-relativistic matter density in the presence of interaction is given by

$$\dot{\rho}_m + 3H\rho_m = -Q \,.$$

For interaction term, $Q = -\alpha_{,\phi}\dot{\phi}\rho_m$, on solving the above equation we get, $\rho_m = \rho_{m_0} e^{\alpha(\phi)-\alpha(\phi_0)} a^{-3}$.

We use these equations to study the universe's evolution in the presence of nonzero interaction and establish the consistency of the model with the latest low redshift observations. The observations used in the analysis are: a) the direct measurements of Hubble parameter (Hz) with observations in the redshift range of $0.070 \leq z \leq 1.965$, b) the baryon acoustic oscillations (BAO) data ($0.106 \leq z \leq 2.36$), c) High-redshift HII Galaxy measurements (HIIG) which spans in a range $0.0088 \leq z \leq 2.42935$, and d) type Ia Supernovae (SN) observations with data points between range $0.05 \leq z \leq 1.4$. To obtain the constraints on model parameters, we use the chi-squared minimization technique, which tells about the goodness of the fit by comparing the observed values of an observable with the theoretically expected values for a specific model (dark energy dark matter interaction model in our case).

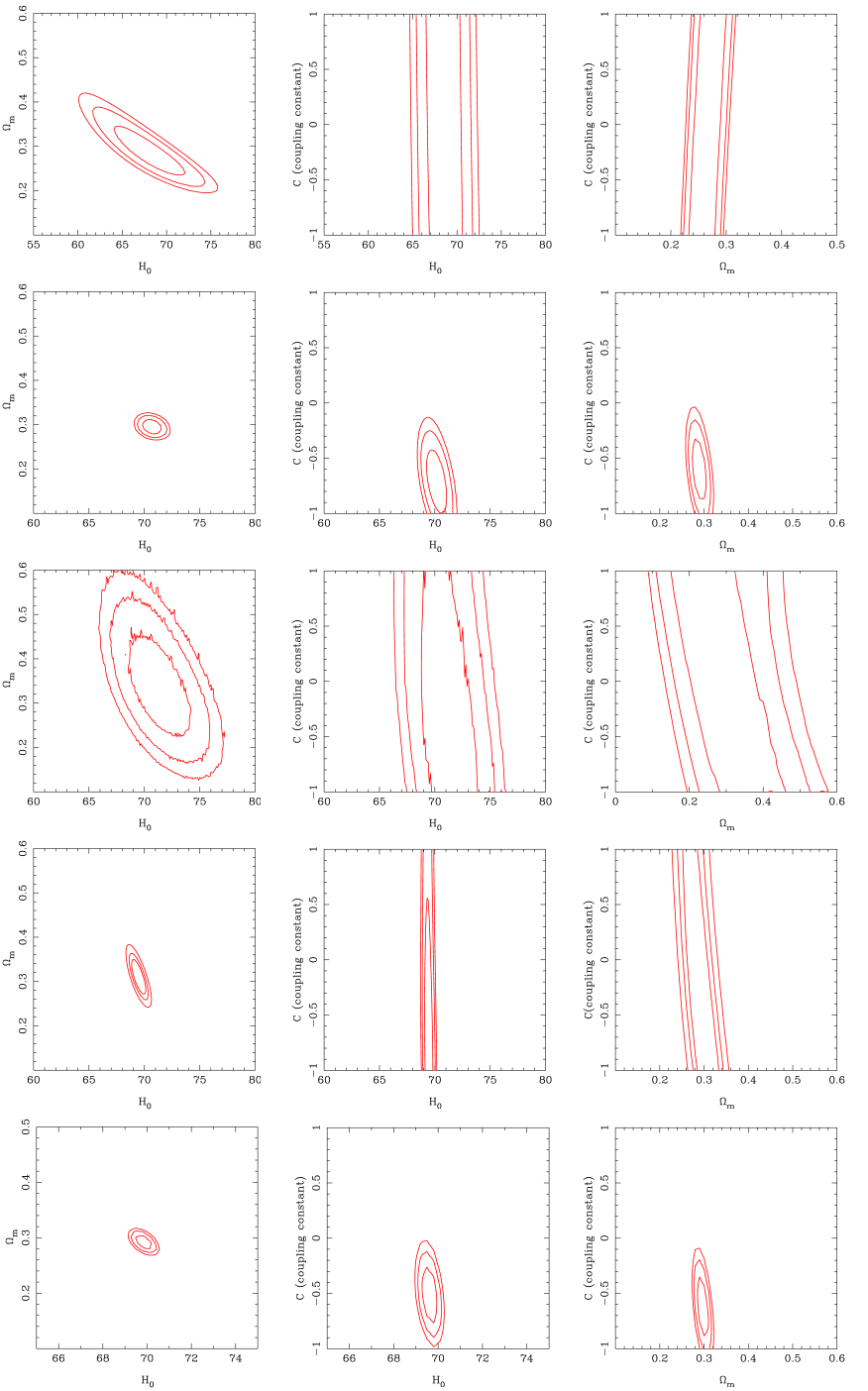

Fig. 1. 1,2,3-σ confidence regions for Hz data (I row), BAO+Hz data (II row), HIIG data (III row), SN+Hz data (IV row) and all four data sets (V row).

3. Observational Constraints

In the analysis, the parameter describing the model are: the Hubble parameter at present (H_0), nonrelativistic matter density parameter (Ω_m), dark energy equation of state parameter at present (w_0), and the interaction strength (C). The priors used in the analysis are given in table below.

Parameter	Lower Limit	Upper Limit
H_0	60.0	80.0
Ω_m	0.1	0.6
w_0	-1.0	1.0
C	-1.0	1.0

We perform the chi-squared minimization technique to obtain the $1, 2, 3 - \sigma$ confidence regions for the four observations we considered in the analysis and provide the results in two-dimensional planes in Fig. 1. We assume $n = 1$ in the analysis and have marginalized over the other parameters to obtain the results in the two-dimensional plane. The results from Hz observation are shown in the first row. The allowed range from Hz data for Ω_m and H_0 parameters are fairly large as compared to the allowed uncertainties obtained from BAO measurements (second row) and SN data (fourth row). On the other hand, the interaction strength parameter C is not constrained by Hz observations, and the entire range is allowed by the observations. BAO+Hz data (second row) provides the tightest constraints on the cosmological parameters, and these observations also obtain the upper limit on interaction strength.

Constraints from HIIG data are presented in the third row (where we have not included the systematic error in the analysis for HIIG data); the HIIG data is unable to constrain the H_0 parameter and provides the largest allowed range for Ω_m among the data sets considered in the analysis. In the fourth row, results from SN+Hz are presented. SN+Hz data also provides narrow constraints on H_0 and Ω_m parameters and gives an upper limit on the interaction strength. Finally, the results from combining the data sets (Hz+BAO+HIIG+SN) are given in row fifth. We find that by performing combined analysis, we get a very narrow range of uncertainties in parameter estimation, and the best fit values of parameters are given by $H_0 = 69.9\ km\ s^{-1}\ Mpc^{-1}$, $\Omega_m = 0.29$, and $C = -0.47$. From the analysis, we find that all the observations are consistent with negative values of C, and the upper on C is given by SN+Hz and BAO+Hz observations which drive the combined results.

We show the results in $\Omega_m - w_0$ plane obtained from Hz (first row, left), BAO+Hz (first row, right), HIIG (the second row, left), and SN+Hz (second row right) observations in Fig. 2. For all the observations, we find that the model is consistent with the cosmological constant model, and BAO+Hz data provides the narrowest

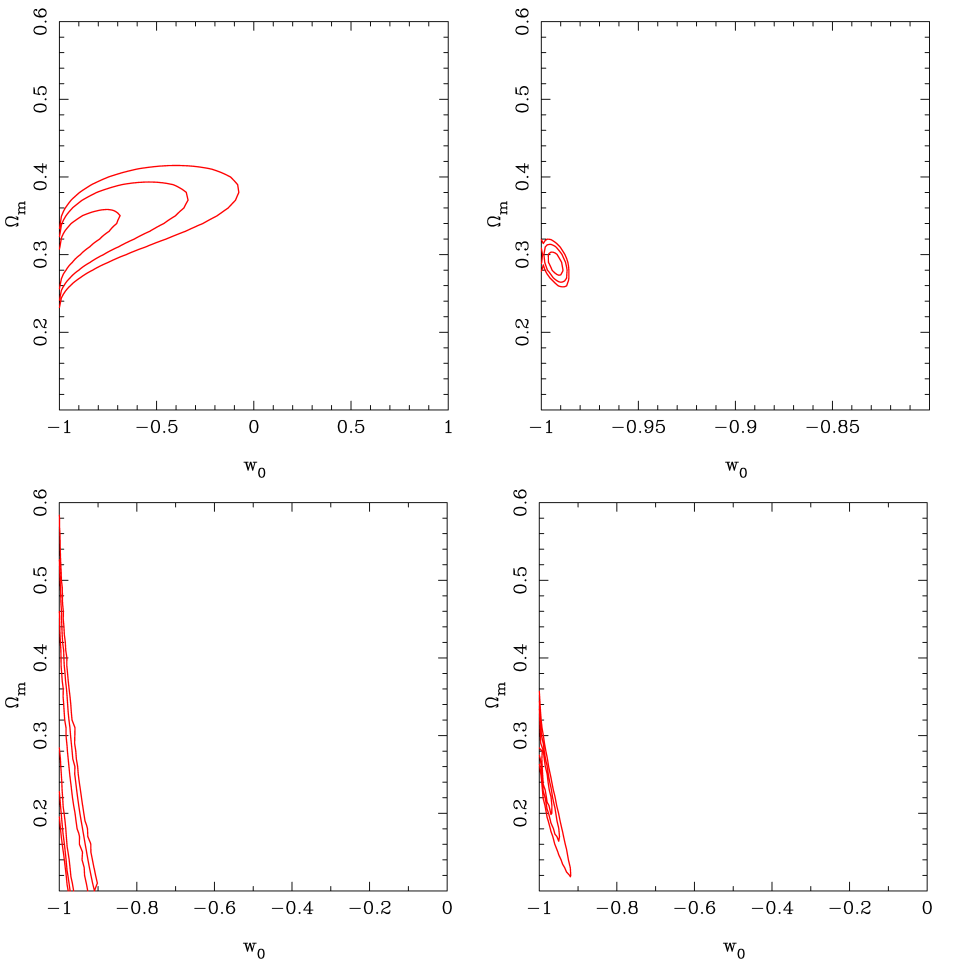

Fig. 2. 1,2,3-σ confidence regions in 'w_0-Ω_m' plane. The first row shows constraints from Hz data (left) and BAO+Hz observations (right). The second row shows constraints from HIIG measurements (left) and SN+Hz observations (right).

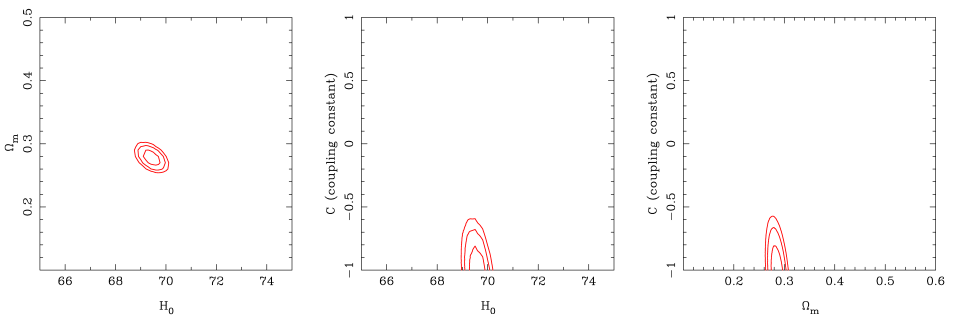

Fig. 3. 1,2,3-σ confidence regions for combined analysis of all four data sets.

constraints on Ω_m and w_0 parameters followed by Sn+Hz measurements. However, Hz data also allows for non-accelerating universe scenarios.

We have also performed the chi-squared analysis for the $n = 2$ case. And we find that the key conclusions from $n = 1$ remain the same that all the observations constrain H_0 to be close to 70 $km\ s^{-1}\ Mpc^{-1}$ and the narrowest constraints are obtained from BAO+Hz and SN+Hz, followed by Hz and HIIG observation. The change in results from individual observations is not significant as we move from $n = 1$ to $n = 2$ case. The only difference worth mentioning is that as n changes from 1 to 2, the contours show a slight shift value of C towards -1, and the model seems to prefer negative values of interaction strength. This preference is more notable in the results from the combined analysis of all the previously mentioned observations. In Fig. 3, we show the 1,2,3-σ confidence regions for combined analysis from all the four data sets considered in the analysis. The effect on Ω_m and H_0 constraints is not significant as we go from $n = 1$ to $n = 2$ case, and the constraints obtained from each dataset are consistent with each other.

Examining the constraints obtained through the evolution of background cosmological equations and using low redshift observations, it is evident that we cannot distinguish between interacting and noninteracting scenarios. Therefore, in the next section, we study the evolution of first-order perturbations in the presence of a nonzero interacting term.

4. Evolution of Perturbations

In this section, we study the evolution of quantities that depends upon the evolution of first-order cosmological perturbations and are related to the observations in current cosmological experiments. The cosmological quantities we discuss are related to structure formation, gravitational lensing and integrated Sachs-Wolfe effect, denoted by δ_m, $\Phi + \Psi$, and $\Phi' + \Psi'$ respectively.

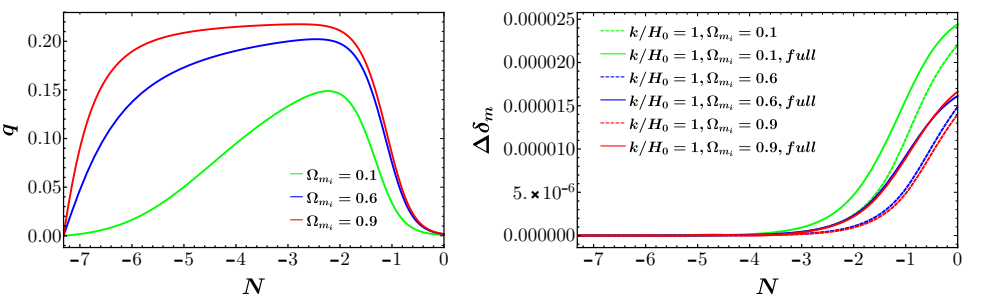

Fig. 4. Evolution of q (left panel) and $\Delta\delta_m$ (right panel) as a function of N with $C = -0.6$.

Structure formation: To study the effect of interaction between dark energy and dark matter on structure formation, we study the evolution of matter density per-

turbation denoted by δ_m, for various length scales. The parameter δ_m is defined as $\delta_m(t,x,y,z) \equiv \frac{\delta\rho_m(t,x,y,z)}{\overline{\rho_m}(t)}$, where $\overline{\rho_m}(t)$ is the mean matter density at time t.

In Fig. 4, the left plot shows the evolution of the scaled interaction term given by $q = \frac{Q}{H^3 M_{Pl}^2}$ as a function of N for different initial values of matter density parameter Ω_m, where $N = ln(a)$ is the number of e-foldings. We see that for a larger value of initial matter density, the contribution of the interaction term is greater and becomes significant at an earlier time than for smaller initial matter density values. The right plot shows the evolution of $\Delta\delta_m = \delta_{m_i} - \delta_{m_{ni}}$ as a function of N. The plot shows the difference in the evolution of matter density perturbations in the interacting and noninteracting models denoted by parameters δ_{m_i} and $\delta_{m_{ni}}$ respectively. The dotted lines are for the case when the perturbed interaction term is neglected, and the solid line is when we consider the perturbed interaction term. The different colors correspond to the different initial values of the matter density parameter. We see that at around $N \sim 2$, the curves deviate from one another, showing that considering the interaction term changes the evolution of matter perturbations, and the maximum change is observed in smaller Ω_{m_i} case. This demonstrates that its possible to detect the signature of dark energy and dark matter interactions in future large scale structure observations.[38–40]

Weak gravitational lensing: The quantity $\Phi + \Phi$ contributes to the weak gravitational lensing effect that is the result of deviation in photon trajectory because of the mass distribution in space. This section discusses the evolution of Φ as in standard cosmology, $\Phi = \Psi$. The evolution of Φ as a function of N is shown in Fig. 5. The plot on the left is for dark energy dark matter interaction scenario with interaction strength $C = -0.6$, and the right plot is for noninteracting scenarios. The different curves correspond to different length scales represented by different values of k. The curves are obtained by evolving the system of equations with the same initial conditions starting at a redshift of $z_i = 1500$. We find that the effect of interaction is clear on the smallest scale considered in the analysis, i.e., at $k/H_0 = 1$. Therefore, we can use the evolution of scalar perturbations to distinguish between the interacting and noninteracting dark energy dark matter scenarios by the future observations of weak gravitational lensing.[41]

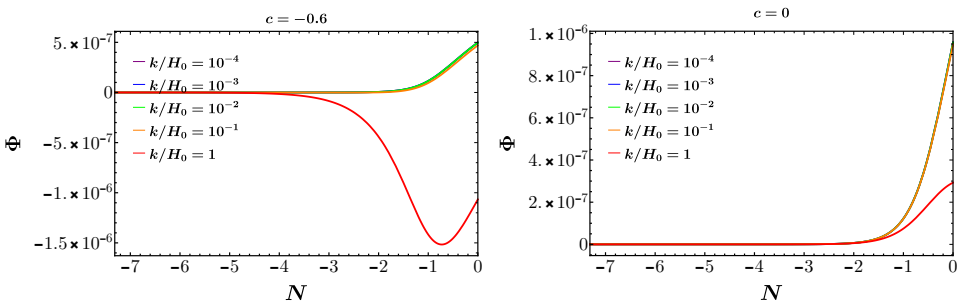

Fig. 5. Evolution of Φ as a function of N. Left: $C = -0.6$, Right: $C = 0$.

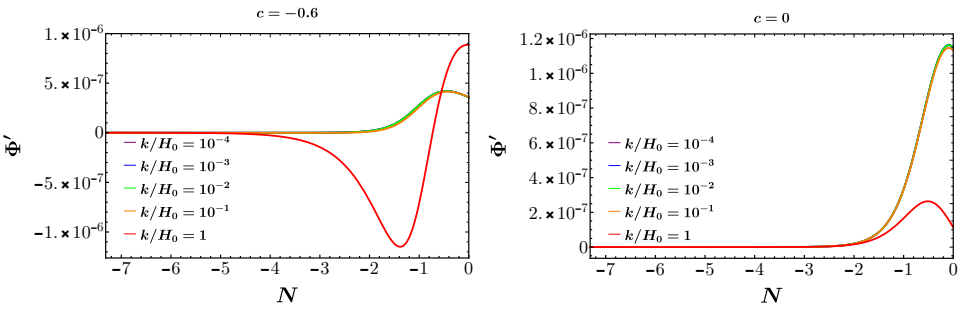

Fig. 6. Evolution of Φ' as a function of N. Left: $C = -0.6$, Right: $C = 0$.

Integrated Sachs-Wolfe effect: This effect manifests in cosmic microwave background radiation anisotropies because of the change in gravitational potential in the path of photons as the photons travel after decoupling from the last scattering surface towards the observer. This effect is given by $\Phi' + \Psi'$, where $'$ denotes the rate of change with respect to conformal time. The change in the evolution of Φ' as a function of N for interacting case with interaction strength $C = -0.6$ (left plot) and noninteracting (right plot) scenarios is given Fig. 6. The different curves correspond to different length scales. The change in the evolution of Φ' because of interaction is observed at $N \sim 3$ where the Φ' is suppressed as compared to the noninteracting scenario. And the maximum change is observed on the smaller scales, and hence, this effect could be observed in the CMB anisotropies. Therefore, using the ISW observations, we can distinguish between interacting and noninteracting scenarios.

5. Conclusion

In this work, we consider a dark energy dark matter interaction model and check the consistency of the model with low redshift observations. In this model, the interaction term is obtained by assuming a one-to-one mapping between the classical field description and the fluid description of the interacting model. We perform the chi-squared minimization technique and obtain the constraints on model parameters. The observations we use in the analysis are direct measurements of Hubble parameter (Hz), baryon acoustic oscillation (BAO) data, measurements of HII galaxies (HIIG), and type Ia supernovae data (SN). We obtain narrow constraints on Hubble parameter H_0, non-relativistic matter density parameter Ω_m, and dark energy equation of state parameter at present w_0. The BAO+Hz and SN+Hz observations provide an upper limit on interaction parameter C. The constraints from these observations are consistent with one another, and the best fit value from all the observations are close to $H_0 \sim 70\ km\ s^{-1}\ Mpc^{-1}$. So there is no tension in the estimated value of H_0 from these observations for the interaction model considered.

The Interaction model is consistent with the abovementioned low redshift observations used in the analysis.

From background analysis, we also observed that it is difficult to distinguish between the interacting and noninteracting models, and therefore we must look at the evolution of perturbations. Therefore, we studied the evolution of first order perturbation quantities such as δ_m, Φ, and Φ' in the interacting and noninteracting case. We find that the evolution of these quantities is modified in the presence of dark energy dark matter interaction terms. Therefore, using the observations of structure formation, weak gravitational lensing, and integrated Sach-Wolfe effect, which depends upon the evolution perturbed quantities mentioned above and carries the signature of the interaction, we can distinguish between the interacting and noninteracting scenarios.

Acknowledgments

The work is partially supported by the ISRO-Respond grant. J.P.J. is supported by CSIR Senior Research Fellowship, India.

References

1. J. P. Johnson, A. Sangwan and S. Shankaranarayanan, Cosmological perturbations in the interacting dark sector: Observational constraints and predictions (2 2021).
2. A. G. Riess *et al.*, Observational evidence from supernovae for an accelerating universe and a cosmological constant, *Astron. J.* **116**, 1009 (1998).
3. S. Perlmutter *et al.*, Measurements of Ω and Λ from 42 high redshift supernovae, *Astrophys. J.* **517**, 565 (1999).
4. D. N. Spergel *et al.*, Wilkinson Microwave Anisotropy Probe (WMAP) three year results: implications for cosmology, *Astrophys. J. Suppl.* **170**, p. 377 (2007).
5. D. M. Scolnic *et al.*, The Complete Light-curve Sample of Spectroscopically Confirmed SNe Ia from Pan-STARRS1 and Cosmological Constraints from the Combined Pantheon Sample, *Astrophys. J.* **859**, p. 101 (2018).
6. N. Aghanim *et al.*, Planck 2018 results. I. Overview and the cosmological legacy of Planck, *Astron. Astrophys.* **641**, p. A1 (2020).
7. N. Aghanim *et al.*, Planck 2018 results. VI. Cosmological parameters, *Astron. Astrophys.* **641**, p. A6 (2020), [Erratum: Astron.Astrophys. 652, C4 (2021)].
8. V. Marra, L. Amendola, I. Sawicki and W. Valkenburg, Cosmic variance and the measurement of the local Hubble parameter, *Phys. Rev. Lett.* **110**, p. 241305 (2013).
9. L. Verde, P. Protopapas and R. Jimenez, Planck and the local Universe: Quantifying the tension, *Phys. Dark Univ.* **2**, 166 (2013).
10. K. C. Wong *et al.*, H0LiCOW – XIII. A 2.4 per cent measurement of H0 from lensed quasars: 5.3σ tension between early- and late-Universe probes, *Mon. Not. Roy. Astron. Soc.* **498**, 1420 (2020).
11. A. G. Riess, S. Casertano, W. Yuan, L. M. Macri and D. Scolnic, Large Magellanic Cloud Cepheid Standards Provide a 1% Foundation for the Determination of the Hubble Constant and Stronger Evidence for Physics beyond ΛCDM, *Astrophys. J.* **876**, p. 85 (2019).

12. P. A. R. Ade *et al.*, Planck 2015 results. XV. Gravitational lensing, *Astron. Astrophys.* **594**, p. A15 (2016).
13. P. A. R. Ade *et al.*, Planck 2015 results. XXVII. The Second Planck Catalogue of Sunyaev-Zeldovich Sources, *Astron. Astrophys.* **594**, p. A27 (2016).
14. K. Kuijken *et al.*, Gravitational Lensing Analysis of the Kilo Degree Survey, *Mon. Not. Roy. Astron. Soc.* **454**, 3500 (2015).
15. S. Joudaki *et al.*, KiDS-450: Testing extensions to the standard cosmological model, *Mon. Not. Roy. Astron. Soc.* **471**, 1259 (2017).
16. S. Joudaki *et al.*, KiDS-450 + 2dFLenS: Cosmological parameter constraints from weak gravitational lensing tomography and overlapping redshift-space galaxy clustering, *Mon. Not. Roy. Astron. Soc.* **474**, 4894 (2018).
17. T. M. C. Abbott *et al.*, Dark Energy Survey year 1 results: Cosmological constraints from galaxy clustering and weak lensing, *Phys. Rev. D* **98**, p. 043526 (2018).
18. E. Di Valentino, A. Melchiorri and O. Mena, Can interacting dark energy solve the H_0 tension?, *Phys. Rev. D* **96**, p. 043503 (2017).
19. W. Yang, A. Mukherjee, E. Di Valentino and S. Pan, Interacting dark energy with time varying equation of state and the H_0 tension, *Phys. Rev. D* **98**, p. 123527 (2018).
20. E. Di Valentino, A. Melchiorri, O. Mena and S. Vagnozzi, Nonminimal dark sector physics and cosmological tensions, *Phys. Rev. D* **101**, p. 063502 (2020).
21. A. Gómez-Valent, V. Pettorino and L. Amendola, Update on coupled dark energy and the H_0 tension, *Phys. Rev. D* **101**, p. 123513 (2020).
22. J. P. Johnson and S. Shankaranarayanan, Cosmological perturbations in the interacting dark sector: Mapping fields and fluids, *Phys. Rev. D* **103**, p. 023510 (2021).
23. J. Simon, L. Verde and R. Jimenez, Constraints on the redshift dependence of the dark energy potential, *Phys. Rev. D* **71**, p. 123001 (2005).
24. D. Stern, R. Jimenez, L. Verde, S. A. Stanford and M. Kamionkowski, Cosmic Chronometers: Constraining the Equation of State of Dark Energy. II. A Spectroscopic Catalog of Red Galaxies in Galaxy Clusters, *he Astrophysical Journal Supplement* **188**, 280 (May 2010).
25. A. L. Ratsimbazafy, S. I. Loubser, S. M. Crawford, C. M. Cress, B. A. Bassett, R. C. Nichol and P. Väisänen, *Mon. Not. Roy. Astron. Soc.* **467**, 3239 (2017).
26. C. Zhang, H. Zhang, S. Yuan, S. Liu, T.-J. Zhang and Y.-C. Sun, Four new observational H(z) data from luminous red galaxies in the Sloan Digital Sky Survey data release seven, *Research in Astronomy and Astrophysics* **14**, 1221 (October 2014).
27. M. Moresco, Raising the bar: new constraints on the Hubble parameter with cosmic chronometers at z $\sim$ 2, *Mon. Not. Roy. Astron. Soc.* **450**, L16 (2015).
28. M. Moresco, L. Pozzetti, A. Cimatti, R. Jimenez, C. Maraston, L. Verde, D. Thomas, A. Citro, R. Tojeiro and D. Wilkinson, A 6% measurement of the Hubble parameter at $z \sim 0.45$: direct evidence of the epoch of cosmic re-acceleration, *JCAP* **05**, p. 014 (2016).
29. A. L. González-Morán, R. Chávez, R. Terlevich, E. Terlevich, F. Bresolin, D. Fernández-Arenas, M. Plionis, S. Basilakos, J. Melnick and E. Telles, Independent cosmological constraints from high-z H ii galaxies, *Mon. Not. Roy. Astron. Soc.* **487**, 4669 (2019).
30. R. Terlevich, E. Terlevich, J. Melnick, R. Chávez, M. Plionis, F. Bresolin and S. Basilakos, On the road to precision cosmology with high-redshift H II galaxies, *Mon. Not. Roy. Astron. Soc.* **451**, 3001 (2015).
31. A. Font-Ribera *et al.*, Quasar-Lyman α Forest Cross-Correlation from BOSS DR11 : Baryon Acoustic Oscillations, *JCAP* **05**, p. 027 (2014).

32. J. E. Bautista *et al.*, Measurement of baryon acoustic oscillation correlations at $z = 2.3$ with SDSS DR12 Lyα-Forests, *Astron. Astrophys.* **603**, p. A12 (2017).
33. M. Ata *et al.*, The clustering of the SDSS-IV extended Baryon Oscillation Spectroscopic Survey DR14 quasar sample: first measurement of baryon acoustic oscillations between redshift 0.8 and 2.2, *Mon. Not. Roy. Astron. Soc.* **473**, 4773 (2018).
34. A. J. Ross, L. Samushia, C. Howlett, W. J. Percival, A. Burden and M. Manera, The clustering of the SDSS DR7 main Galaxy sample – I. A 4 per cent distance measure at $z = 0.15$, *Mon. Not. Roy. Astron. Soc.* **449**, 835 (2015).
35. F. Beutler, C. Blake, M. Colless, D. H. Jones, L. Staveley-Smith, L. Campbell, Q. Parker, W. Saunders and F. Watson, The 6dF Galaxy Survey: baryon acoustic oscillations and the local Hubble constant, *Mon. Not. Roy. Astron. Soc.* **416**, 3017 (October 2011).
36. S. Alam *et al.*, The clustering of galaxies in the completed SDSS-III Baryon Oscillation Spectroscopic Survey: cosmological analysis of the DR12 galaxy sample, *Mon. Not. Roy. Astron. Soc.* **470**, 2617 (2017).
37. M. Betoule *et al.*, Improved cosmological constraints from a joint analysis of the SDSS-II and SNLS supernova samples, *Astron. Astrophys.* **568**, p. A22 (2014).
38. L. Amendola *et al.*, Cosmology and fundamental physics with the Euclid satellite, *Living Rev. Rel.* **21**, p. 2 (2018).
39. R. Maartens, F. B. Abdalla, M. Jarvis and M. G. Santos, Overview of Cosmology with the SKA, *PoS* **AASKA14**, p. 016 (2015).
40. M. P. van Haarlem, M. W. Wise, A. W. Gunst, G. Heald, J. P. McKean, J. W. T. Hessels, A. G. de Bruyn, R. Nijboer, J. Swinbank, R. Fallows, M. Brentjens, A. Nelles, R. Beck, H. Falcke, R. Fender, J. Hörandel, L. V. E. Koopmans, G. Mann, G. Miley, H. Röttgering, B. W. Stappers, R. A. M. J. Wijers, S. Zaroubi, M. van den Akker, A. Alexov, J. Anderson, K. Anderson, A. van Ardenne, M. Arts, A. Asgekar, I. M. Avruch, F. Batejat, L. Bähren, M. E. Bell, M. R. Bell, I. van Bemmel, P. Bennema, M. J. Bentum, G. Bernardi, P. Best, L. Bîrzan, A. Bonafede, A. J. Boonstra, R. Braun, J. Bregman, F. Breitling, R. H. van de Brink, J. Broderick, P. C. Broekema, W. N. Brouw, M. Brüggen, H. R. Butcher, W. van Cappellen, B. Ciardi, T. Coenen, J. Conway, A. Coolen, A. Corstanje, S. Damstra, O. Davies, A. T. Deller, R. J. Dettmar, G. van Diepen, K. Dijkstra, P. Donker, A. Doorduin, J. Dromer, M. Drost, A. van Duin, J. Eislöffel, J. van Enst, C. Ferrari, W. Frieswijk, H. Gankema, M. A. Garrett, F. de Gasperin, M. Gerbers, E. de Geus, J. M. Grießmeier, T. Grit, P. Gruppen, J. P. Hamaker, T. Hassall, M. Hoeft, H. A. Holties, A. Horneffer, A. van der Horst, A. van Houwelingen, A. Huijgen, M. Iacobelli, H. Intema, N. Jackson, V. Jelic, A. de Jong, E. Juette, D. Kant, A. Karastergiou, A. Koers, H. Kollen, V. I. Kondratiev, E. Kooistra, Y. Koopman, A. Koster, M. Kuniyoshi, M. Kramer, G. Kuper, P. Lambropoulos, C. Law, J. van Leeuwen, J. Lemaitre, M. Loose, P. Maat, G. Macario, S. Markoff, J. Masters, R. A. McFadden, D. McKay-Bukowski, H. Meijering, H. Meulman, M. Mevius, E. Middelberg, R. Millenaar, J. C. A. Miller-Jones, R. N. Mohan, J. D. Mol, J. Morawietz, R. Morganti, D. D. Mulcahy, E. Mulder, H. Munk, L. Nieuwenhuis, R. van Nieuwpoort, J. E. Noordam, M. Norden, A. Noutsos, A. R. Offringa, H. Olofsson, A. Omar, E. Orrú, R. Overeem, H. Paas, M. Pandey-Pommier, V. N. Pandey, R. Pizzo, A. Polatidis, D. Rafferty, S. Rawlings, W. Reich, J. P. de Reijer, J. Reitsma, G. A. Renting, P. Riemers, E. Rol, J. W. Romein, J. Roosjen, M. Ruiter, A. Scaife, K. van der Schaaf, B. Scheers, P. Schellart, A. Schoenmakers, G. Schoonderbeek, M. Serylak, A. Shulevski, J. Sluman, O. Smirnov, C. Sobey, H. Spreeuw, M. Steinmetz, C. G. M. Sterks, H. J. Stiepel, K. Stuurwold, M. Tagger,

Y. Tang, C. Tasse, I. Thomas, S. Thoudam, M. C. Toribio, B. van der Tol, O. Usov, M. van Veelen, A. J. van der Veen, S. ter Veen, J. P. W. Verbiest, R. Vermeulen, N. Vermaas, C. Vocks, C. Vogt, M. de Vos, E. van der Wal, R. van Weeren, H. Weggemans, P. Weltevrede, S. White, S. J. Wijnholds, T. Wilhelmsson, O. Wucknitz, S. Yatawatta, P. Zarka, A. Zensus and J. van Zwieten, LOFAR: The LOw-Frequency ARray, *Astronomy & Astrophysics* **556**, p. A2 (August 2013).

41. H. Hildebrandt *et al.*, KiDS-450: Cosmological parameter constraints from tomographic weak gravitational lensing, *Mon. Not. Roy. Astron. Soc.* **465**, p. 1454 (2017).